atmosphere

MDPI

Article

Numerical Simulations of the Impacts of Mountain on Oasis Effects in Arid Central Asia

Miao Zhang [1,2,3,4,5], Geping Luo [1,*], Rafiq Hamdi [6,7], Yuan Qiu [1,3], Xinxin Wang [1,3], Philippe De Maeyer [2,4] and Alishir Kurban [1,4]

1 State Key Laboratory of Desert and Oasis Ecology, Xinjiang Institute of Ecology and Geography, Chinese Academy of Sciences, No. 818 South Beijing Road, Urumqi 830011, China; miaomiaozpb@163.com (M.Z.); qiuyuan.cas@gmail.com (Y.Q.); wangxinxin0803@gmail.com (X.W.); alishir@ms.xjb.ac.cn (A.K.)
2 Department of Geography, Ghent University, Krijgslaan 281, S8, B-9000 Ghent, Belgium; philippe.demaeyer@ugent.be
3 University of the Chinese Academy of Sciences, Beijing 100049, China
4 Sino-Belgian Joint Laboratory for Geo-information, Ghent University, B-9000 Ghent, Belgium
5 Sino-Belgian Joint Laboratory for Geo-information, Xinjiang Institute of Ecology and Geography, Urumqi 830011, China
6 Royal Meteorological Institute, Avenue Circulaire 3, B-1180 Brussels, Belgium; rafiq.hamdi@meteo.be
7 Department of Physics and Astronomy, Ghent University, B-9000 Ghent, Belgium
* Correspondence: luogp@ms.xjb.ac.cn; Tel.: +86-991-7823127; Fax: +86-991-7885320

Received: 15 August 2017; Accepted: 30 October 2017; Published: 1 November 2017

Abstract: The oases in the mountain-basin systems of Central Asia are extremely fragile. Investigating oasis effects and oasis-desert interactions is important for understanding the ecological stability of oases. However, previous studies have been performed only in oasis-desert environments and have not considered the impacts of mountains. In this study, oasis effects were explored in the context of mountain effects in the northern Tianshan Mountains (NTM) using the Weather Research and Forecasting (WRF) model. Four numerical simulations are performed. The *def* simulation uses the default terrestrial datasets provided by the WRF model. The *mod* simulation uses actual terrestrial datasets from satellite products. The *non-oasis* simulation is a scenario simulation in which oasis areas are replaced by desert conditions, while all other conditions are the same as the *mod* simulation. Finally, the *non-mountain* simulation is a scenario simulation in which the elevation values of all grids are set to a constant value of 300 m, while all other conditions are the same as in the *mod* simulation. The *mod* simulation agrees well with near-surface measurements of temperature, relative humidity and latent heat flux. The Tianshan Mountains exert a cooling and wetting effects in the NTM region. The oasis breeze circulation (OBC) between oases and the deserts is counteracted by the stronger background circulation. Thus, the self-supporting mechanism of oases originating from the OBC plays a limited role in maintaining the ecological stability of oases in this mountain-basin system. However, the mountain wind causes the "cold-wet" island effects of the oases to extend into the oasis-desert transition zone at night, which is beneficial for plants in the transition region.

Keywords: oasis effects; mountain-basin system; oasis breeze circulation; mountain-valley wind; WRF; Central Asia arid area

1. Introduction

Oases are common in the deserts of arid areas [1–4], especially in the hinterland of arid Central Asia (CA). The formation of an oasis in this region is closely related to the geomorphic characteristics of high mountain-basin systems, because the melting of snow and glaciers and the precipitation in tall mountain ranges provide necessary water resources for oasis survival and

development in these mountain-basin systems [5]. Accordingly, watersheds represent a basic unit in this mountain-oasis-desert system (MODS). The Northern Tianshan Mountains (NTM) is one of the typical geomorphic regions of CA and consists of a large number of complex MODSs. Although oases account for only a small proportion of the land surface (e.g., 4–5% in Xinjiang, a typical region in the hinterlands of Central Asia), more than 90% of the local population and >95% of the socioeconomic wealth are concentrated in oases [6]. Thus, oases play a vital role in social and economic development. Since the 1950s, the region has experienced distinct and intense land reclamation, characterized mainly by oasis expansion. The total oasis area has expanded to 4.23 times its original value (from 121.0 $\times$ 10^4 ha in 1949 to 512.5 $\times 10^4$ ha in 2010). As a result, a series of ecological problems have appeared due to the limited water and soil conditions [7–9], such as desertification and soil salinization [10,11]. These problems have hindered the sustainable development of the oases.

Oasis effects are thought to play an important role in maintaining the existence of oases over time. In the recent literature, several studies based on both field observations and numerical simulations have focused on the exchanges of water and energy between oases and the surrounding deserts [12–15]. The differences in the geographical and ecological characteristics between oasis areas and desert areas result in significant differences in their energy budgets, create exchanges of momentum and water vapor and affect the amounts of heat and moisture released to the atmosphere within the convective boundary layer. During daytime, solar radiation heats the desert surface and rapidly increases the near-surface temperatures over desert areas. In contrast, the temperature over oases is lower due to the intense level of evaporation occurring in oases [16]. At the same time, the humidity over oases is higher than that over the desert. The air density and pressure in the near-surface layer over the desert are lower than over the oasis, thereby causing cold moist air to flow from the oasis to the desert, resulting in a moisture inversion over the desert [17]. At higher elevation, the hot dry air over the desert flows toward the oasis, resulting in the oasis becoming a cold, wet island capped by warm, dry air. This phenomenon has been observed to create a temperature inversion layer and negative sensible heat fluxes over oases [12,18–20] and is known as the "oasis effects" [16]. The water and heat differences between the oasis and the desert cause local atmospheric circulation patterns, called oasis breeze circulation (OBC). Recent numerical simulations of OBC have been performed using regional climate models coupled to sophisticated land surface schemes, such as the fifth-generation Penn State / National Center for Atmospheric Research (NCAR) Mesoscale Model (MM5) or the Weather Research and Forecasting (WRF) model [6,17,21–28]. These studies have improved our understanding of the mechanisms and processes associated with the oasis-desert interactions. The conception of the "self-supporting mechanism of oasis" has been proposed based on OBC. Specifically, the downdrafts over an oasis decrease evaporation within the oasis, whereas the updrafts over the desert areas adjacent to the oasis act as a wall that hinders the transfer of cold, wet air to the dry surrounding desert [16,28]. Thus, the OBC helps to maintain the ecological stability of oases by reducing the exchanges of heat and moisture between oases and the surrounding desert areas.

However, an oasis cannot survive without a supply of water from the nearby large mountains in a MODS. Therefore, studies should explore the oasis effects, i.e., the oasis-desert interactions, under the impacts of these surrounding mountains rather than focusing only on the oasis and desert areas [6,17,21–28]. Failing to consider the impacts of the mountains may result in an incorrect or incomplete understanding of the oasis-desert interactions within a MODS. For example, what are the spatial patterns of water and heat throughout MODS? Do intense mountain-valley winds occur within current MODSs [29,30]? Finally, how does the mountain-valley wind, if present, impact the oasis effects and OBC? The answers to these questions are not clear and deserve additional and comprehensive investigation. Since, once OBC ceases to operate within a MODS, the self-supporting mechanism of oasis originated from OBC will disappear and the water vapor over the oasis may flow into the surrounding deserts. Consequently, the oasis will become drier and drier, perhaps resulting in a vicious cycle of water deficiency and desertification [6]. Accordingly, answering the above questions is essential, both theoretically and practically, to the sustainable development and ecological stability

of oases and will provide useful information for further investigating the impact of oasis expansion on regional climate changes [31] under global warming.

The WRF model coupled to the sophisticated land surface scheme Noah has been used to simulate regional climates over the past 10 years [32,33]. The WRF model is sensitive to land surface properties [34,35], especially primary parameters such as land cover (LC) and secondary parameters such as the green vegetation fraction (GVF), the leaf area index (LAI) and albedo, which can be determined from the LC. However, the default values of these parameters are usually from the outdated 1992–1993 Advanced Very High Resolution Radiometer (AVHRR) dataset. Realistic representation of these land surface properties is necessary to improve WRF-based simulations over complex areas, such as MODSs [36]. In this study, actual LC, albedo, LAI and GVF data from the MODerate Resolution Imaging Spectroradiometer (MODIS) products are used.

Our ultimate goals in this paper are to realistically depict the temperature, humidity and circulation patterns of a complex MODS and to describe the impacts of mountain on oasis effects within MODS in Central Asia using the WRF model. The paper is structured as follows. Section 2 presents a description of the study area, the datasets used in this work, the WRF model and the design of the experiments performed here. Section 3 presents the results of the simulations. Section 4 offers a discussion and identifies avenues for future investigation. The final section summarizes the findings of this study.

2. Experiments

2.1. Study Area

In this study, CA includes Xinjiang Province in China and five nations of Kazakhstan, Kyrgyzstan, Tajikistan, Turkmenistan and Uzbekistan [37,38]. CA is controlled by both the westerly circulation in the middle-high latitudes and the polar air mass [39] and experiences an arid continental climate with scarce and concentrated rainfall (less than 250 mm in the basin regions and 900 mm in the upwind mountains). CA contains many of the highest-altitude mountains and basins in the world. Due to the unique topography of this area, the runoff from the melting of snow, glaciers and precipitation that occurs in the mountainous areas [39] represents the main sources of water for inland basins in the mountain-basin systems. The limited abundance of runoff promotes the development of relatively high-productivity oasis systems in the mountain-basin systems by irrigation (runoff flows into the oasis then disappears in the desert areas due to strong evapotranspiration and groundwater recharge). Because of the elevation differences and the importance of oases, the mountain-basin landscapes can be artificially divided into three regions: mountainous areas, oasis areas and desert areas [5].

The Tianshan Mountains, which are located in the hinterland of CA, act as the "water tower of Central Asia" [40]. The NTM is used as the study area in this paper because it includes many the special characteristics of MODSs (Figure 1a) and is a microcosm of the terrain and climate of CA. Furthermore, the periphery of the NTM region has experienced intense human activity, such as oasis expansion, urbanization and resulting desertification over the past 60 years [41,42]. The oases in the NTM region developed in the groundwater overflow zone between the foothills and the surrounding Gurban Tonggut desert (Figure 1b). The simulation region, spanning a total area of 260,400 km^2, covers the whole NTM region, thus capturing the mountain effects.

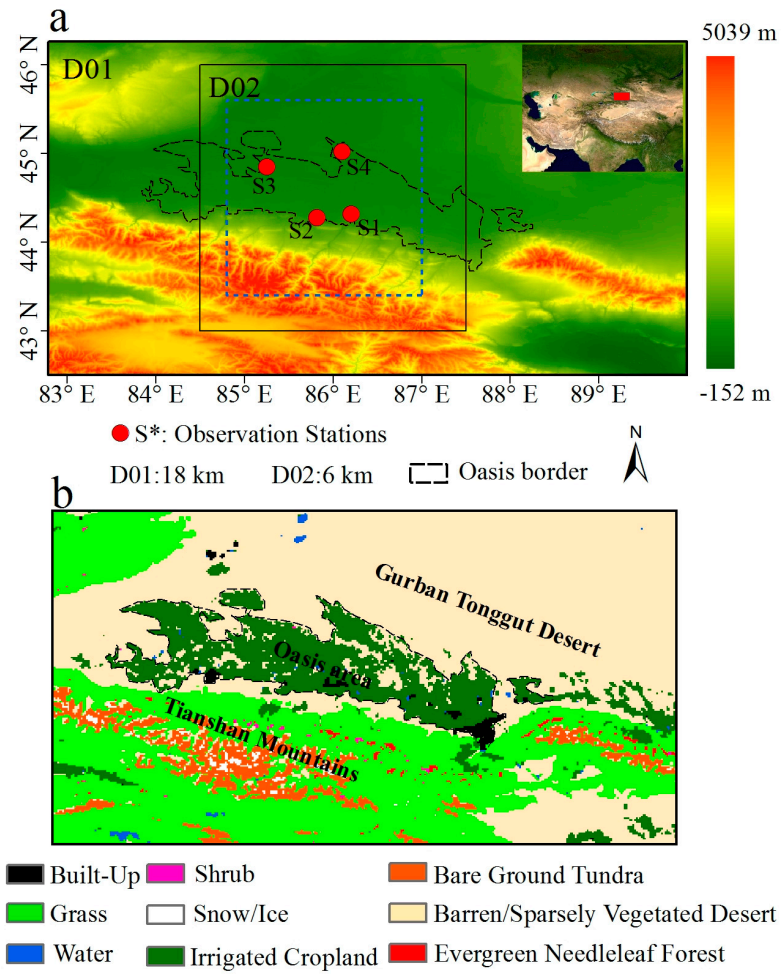

Figure 1. Topography (**a**) and land cover (**b**) of the study area in 2012 and the Weather Research and Forecasting (WRF) simulation domains (blue dotted line in (**a**) shows the horizontal extent of the analyzed area in the subsequent figures).

2.2. Model Description and Configuration

The WRF model is an advanced mesoscale numerical weather prediction system designed for both climate research and numerical weather prediction [43]. It was developed jointly by the NCAR and the National Centers for Environmental Prediction (NCEP). The Noah land surface model was also developed through multi-institutional collaborative efforts among NCEP, NCAR, the U.S. Air Force Weather Agency, NASA and the university community [44–46]. The Noah model, which has been implemented in the WRF and MM5 models [47], provides reasonable diurnal variations of surface heat fluxes as surface boundary conditions for coupled models, as well as correct seasonal evolution patterns of soil moisture in the context of long-term data assimilation systems [32,48]. In this study, WRF version 3.6 coupled with Noah was used in our simulations.

For this study, the model was configured for fine-scale simulation with two-way nested domains (D01 and D02, Figure 1a). The outer domain (D01) and the inner domain (D02) have grid spacing of approximately 18 km and 6 km, respectively, in the horizontal direction. The inner domain (D02) is our main region of interest. It covers a total area of approximately 330.78 km × 244.23 km and contains 50 × 50 grids cells. The ERA-Interim reanalysis data provides the initial and lateral boundary conditions for simulations at 6-h intervals. The simulation results from domain D01 are stored hourly and provide hourly lateral boundary conditions for D02. Part of the grids points in each side of D02 are discarded and the remaining points are used as the analysis (blue dotted line in Figure 1a). The initial

soil moisture and the soil boundary temperatures are derived from the forcing data; however, the soil moisture levels of the oases and desert areas are adjusted using observations (for details, see Section 2.4). Both domains are run with 35 unevenly spaced full eta levels with 15 levels below a height of 5 km above the ground surface. The model's upper surface was fixed at 50 hPa. A series of analyses that examine the model's sensitivity to the different parameterizations of the physical atmospheric processes operating over the study region was previously performed by Qiu et al. [49]. In this study, we use the optimal WRF configurations. Namely, planetary boundary layer processes are resolved using the Yonsei University scheme [50], the microphysics are simulated using the WRF Single Moment-3 scheme [51], the cumulus clouds are simulated using the Kain-Fritsch Scheme [52] and the Community Atmospheric Model scheme is used to calculate the longwave and shortwave radiation [53].

2.3. Data

2.3.1. Forcing Data and In Situ Measurements

The latest global atmospheric reanalysis product ERA-Interim [54] provides the initial and lateral boundary conditions for the WRF simulation in this paper. These data were produced by the European Centre for Medium-Range Weather Forecasts. We employ the fields describing geo-potential, relative humidity, temperature, the U and V wind components at 30 pressure levels and surface forcing parameters, including the 10-m U wind, the 10-m V wind, the 2-m dew point temperature, the 2-m temperature, the mean sea level pressure, the sea surface temperature, the sea-ice cover, the skin temperature, the snow density, the snow depth, the soil temperature and the soil water content in 4 different layers. The spatial resolution of the dataset is $0.75^\circ \times 0.75^\circ$ and the data are reported at 6-h intervals.

In situ observations from four meteorological stations within domain D02 are used to validate the simulation results and these four stations are distributed in oasis areas with diverse LC types, including irrigated crops, urban areas and combinations of both (Table 1). Hourly in situ readings of the 2-m air temperature, the 2-m relative humidity and the 10-m wind speed and direction from four meteorological stations are used to validate the simulation results. In addition, observations of latent heat and downward shortwave and longwave radiation from an eddy covariance system at station S2 are also used. Due to a damaged radiation sensor, observations of sensible heat flux are not available.

Table 1. Station information and parameters measured at each station.

Station	Longitude (°E)	Latitude (°N)	Altitude (m)	Land Cover Type	Time Interval	Parameters
S1	86.20	44.32	473.10	Crop/Urban	Hourly	T2, RH, W_S, W_D
S2	85.82	44.28	469.30	Crop	Hourly	T2, RH, LE, SW, LW, W_S, W_D
S3	85.25	44.85	338.10	Crop/Desert	Hourly	T2, RH, W_S, W_D
S4	86.10	45.02	347.80	Crop	Hourly	T2, RH, W_S, W_D

T2 represents the 2-m air temperature; RH represents the 2-m relative humidity; LE represents the latent heat flux; W_S and W_D represent the wind speed and direction at 10 m, respectively; SW and LW represent downward shortwave and longwave radiation.

2.3.2. Actual Land Surface Parameters

The default LC data used in the WRF model were originally provided by the U.S. Geological Survey (USGS) and were derived from AVHRR data from 1992 to 1993 [28]. In these data, the land surface is assigned to 24 different LC categories or 19 categories derived from MODIS data for January 2001 to December 2001 [55]. The GVF, LAI and albedo datasets used in the default WRF configuration are based on multi-year averages of monthly maps derived from AVHRR satellite data from 1985 to 1991 [33]. The outdated datasets used in the WRF model (i.e., the default LC, albedo, LAI and GVF datasets) limit its ability to accurately represent land conditions over heterogeneous and complex ground surfaces due to the underestimations of the spatial heterogeneity in LC and the associated land surface properties [34,35].

In this study, we converted an actual LC dataset with a hierarchical classification system (Table S1) into the USGS classification system used in the WRF model [56], based on the corresponding relations shown in Table S2. The actual LC data were generated by the Xinjiang Institute of Ecology and Geography (XIEG), Chinese Academy of Sciences, based on Landsat images and a 1:1,000,000 scale topographic map [57]. The default albedo, LAI and GVF provided by the WRF model have been replaced with the actual MODIS products MCD43A4, MYD15A2 and a GVF dataset computed from MOD13A2 [44,47,58], respectively. These products were downloaded from https://modis.gsfc.nasa.gov/data and correspond to 3 July 2012 and the strip numbers h23v04 and h24v04. We reprocessed these products using the same coordinate systems and resolutions as in the numerical simulations (the details are provided in Sections 1–4 of the Supplementary Materials).

2.4. Experimental Design

Four simulations were conducted as follows. (i) The *def* simulation uses the default LC, GVF, LAI, albedo datasets provided by the WRF model; (ii) In the *mod* simulation, the default LC, albedo, LAI and GVF datasets are updated using the MODIS products mentioned in Section 2.3.2; (iii) The *non-oasis* simulation is a sensitivity simulation in which the oasis areas are replaced with desert conditions and the other conditions are the same as in the *mod* simulation; (iv) Finally, the reference *non-mountain* simulation involves setting the elevation value of the grid cells to a constant value of 300 m, while the other conditions are the same as in the *mod* simulation. The differences between the *def* simulation and the *mod* simulation are used to examine the performance of the WRF model using actual biophysical parameters. The differences between the *mod* simulation and the *non-oasis* simulation and the differences between the *mod* simulation and the *non-mountain* simulation were used to quantitatively investigate the effects of oases and mountains, respectively, on temperature, humidity and circulation features within the complete MODS.

All of the experimental simulations are initialized during the period of the most vigorous vegetation growth and extend from 00:00 UTC on 1 July 2012, to 18:00 UTC on 31 July 2012. Generally, in the absence of accurate, gridded initial soil moisture conditions, a spin-up period is needed to allow the soil moisture within Noah to approach equilibrium with the hydrological cycle [32]. The optimal spin-up period for any particular application is uncertain and may require simulations of considerable length, as years may be required to reach equilibrium [59]. In this study, the soil moisture values of the oasis and desert areas are initialized via interpolation from observed soil moistures data from similar oasis and desert regions referenced in a previous paper [28] (Table 2). In addition, also following similar previous simulations of mesoscale water, surface energy and circulation processes [6,21,26], the first 15 days of the simulations are skipped as spin-up to enable the soil moisture of the other land use types in the MODS to reach relative equilibrium. The simulation results covering the periods from 19:00 UTC on 15 July 2012, to 18:00 UTC on 20 July 2012 (i.e., from 00:00 Beijing time on 16 July to 23:00 Beijing time on 20 July), are used for analysis. This 5-day period is characterized by anticyclonic and clear-sky conditions; thus, the effects of cloud distribution are excluded from the results (not shown). All of the spatial patterns of temperature, humidity and circulation during the daytime and nighttime represent the average of the simulation results over these 5 days.

Table 2. Soil moisture values for the oasis and desert areas in the four Noah soil layers [28].

Land Use Type	Noah Soil Layer	Soil Moisture (cm^3 cm^{-3})
Oasis	0–10 cm	0.38 (at 5 cm)
	10–40 cm	0.47 (at 25 cm)
	40–100 cm	0.33 (at 70 cm)
	100–200 cm	0.26 (at 150 cm)
Desert	0–10 cm	0.07 (at 5 cm)
	10–40 cm	0.10 (at 25 cm)
	40–100 cm	0.05 (at 70 cm)
	100–200 cm	0.06 (at 150 cm

3. Results and Analysis

3.1. Comparison of Actual LC, Albedo, LAI and GVF Data and the Corresponding Default Datasets

We examined the differences between the actual LC dataset and the default values during the analysis period (Figure 2a,b). Large urban areas and croplands in the NTM can be clearly observed in the actual LC dataset (Figure 2b)—however, these features are absent in the default dataset (Figure 2a), which instead displays large areas of scrubland and grassland. The default LC dataset is based on AVHRR satellite data from 1992 to 1993 [28]; however, the urban areas and croplands are much larger within the current study area, due to the overexploitation of water and soil resources over the past 20 years. The actual albedo values are generally higher than the default values, which were extracted from multi-year climatological monthly albedo levels [60], with an approximate value of 0.05. Several reasons may underlie these differences [61]. The larger albedo values observed over the oasis areas in the actual dataset may be attributed to severe salinization [62,63] and considerable use of plastic-mulch [64], which have developed in the study area (Figure 2c,d).The differences in the LAI and the GVF between the actual and the default datasets are shown in Figure 2e–h, respectively. Substantial differences are evident within the oasis areas. The LAI values in default dataset range from 0.2 to 1.3, whereas the actual LAI values are generally higher and range from 0.8 to 5. The GVF values range from 15% to 55% in the default dataset (Figure 2g) and from 25% to 92% in the actual image (Figure 2h). The differences within the desert areas are much less noticeable, although slight differences occur near the northern border of the oasis.

3.2. Simulation Evaluation

Figure 3 shows a comparative analysis of the observed and simulated 2-m air temperature (T2), 2-m relative humidity (RH) and latent heat flux (LE) over the oasis surface. The *mod* simulation is closer to the observations than the *def* simulation. The LE computed from the *mod* simulation over the oasis surface provides a much better representation of the peak values and correctly reproduces the overall shape of the observed value.

The mean LE value at the daily maximum from the *mod* simulation is approximately 400 W/m^2, which is two times greater than that of the *def* simulation (Figure 3c). The *mod* LE values are closer to the observations and the mean bias (modeled values minus observations) is up to 40.6 W/m^2 smaller than those of the *def* simulation over the whole period (not shown). Figure 4 compares the mean bias error (MBE), root mean square error (RMSE) and the Pearson correlation coefficient (r) computed from the *mod* and *def* simulations for T2 and RH. For the four sites, the *mod* simulation is clearly closer to the observed values and is associated with significant reductions in the MBE and the RMSE (the *p*-value is less than 0.01) and a significant increase in the Pearson correlation coefficient (the *p*-value is less than 0.01). The performance of the WRF model in the *mod* simulation shows considerable improvements due to the updates of the LC, albedo, LAI and GVF datasets. In fact, the bias in T2 is corrected to approximately 0.3–2.4 °C and that of RH is corrected to 1.9–12.9% in the *mod* simulation.

Note that the reductions in the biases associated with T2, RH and LE are larger at stations S2 and S4 than at the other two locations shown in Figure 3. This pattern occurs because the actual LAI and GVF values at S2 and S4 improved to a much greater degree than those at the other two sites. Specifically, the LAI values at S2 and S4 changed from 1.08 and 0.52 to 4.8 and 3.0, respectively and the GVF values at S2 and S4 changed from 36.6% and 13.5% to 84.7% and 82.15%, respectively (Figure 2g,h). The LC types at S2 and S4 are homogenous cropland but those at S1 and S3 include cropland combined with urban areas (S1) or desert areas (S3), respectively. As a result, more consistent trends and similar magnitudes of T2, RH and LE are observed at the four stations in the *mod* simulation than in the *def* simulation, as shown in Figure 2. This validation indicates that the simulated temperature, humidity and latent heat flux trends obtained from the *mod* simulation are consistent with the observations and realistically represent the water and heat conditions of the oasis surface.

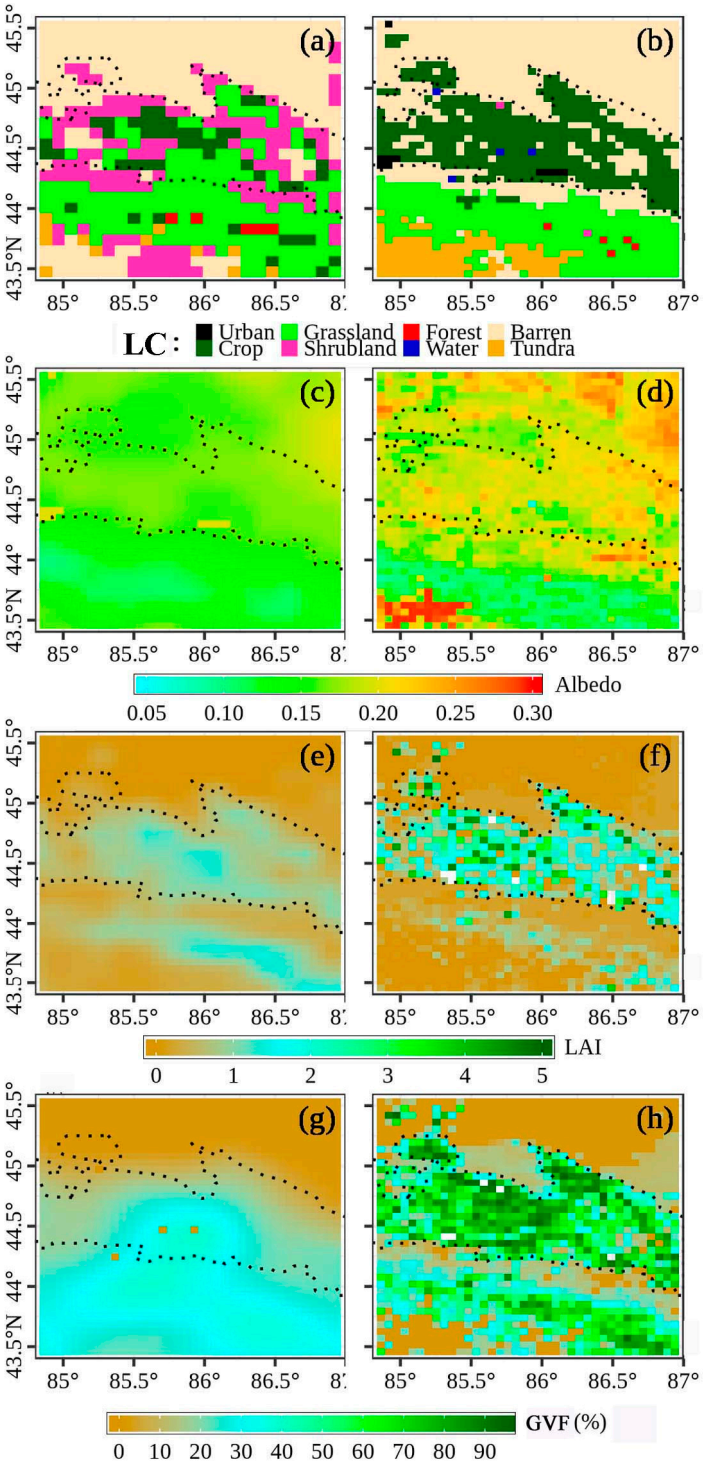

Figure 2. Comparison of (**a**) default LC, (**c**) albedo, (**e**) LAI and (**g**) GVF datasets and the corresponding actual datasets (**b**,**d**,**f**,**h**). From top to bottom: land cover (LC), albedo, leaf area index (LAI) and green vegetation fraction (GVF).

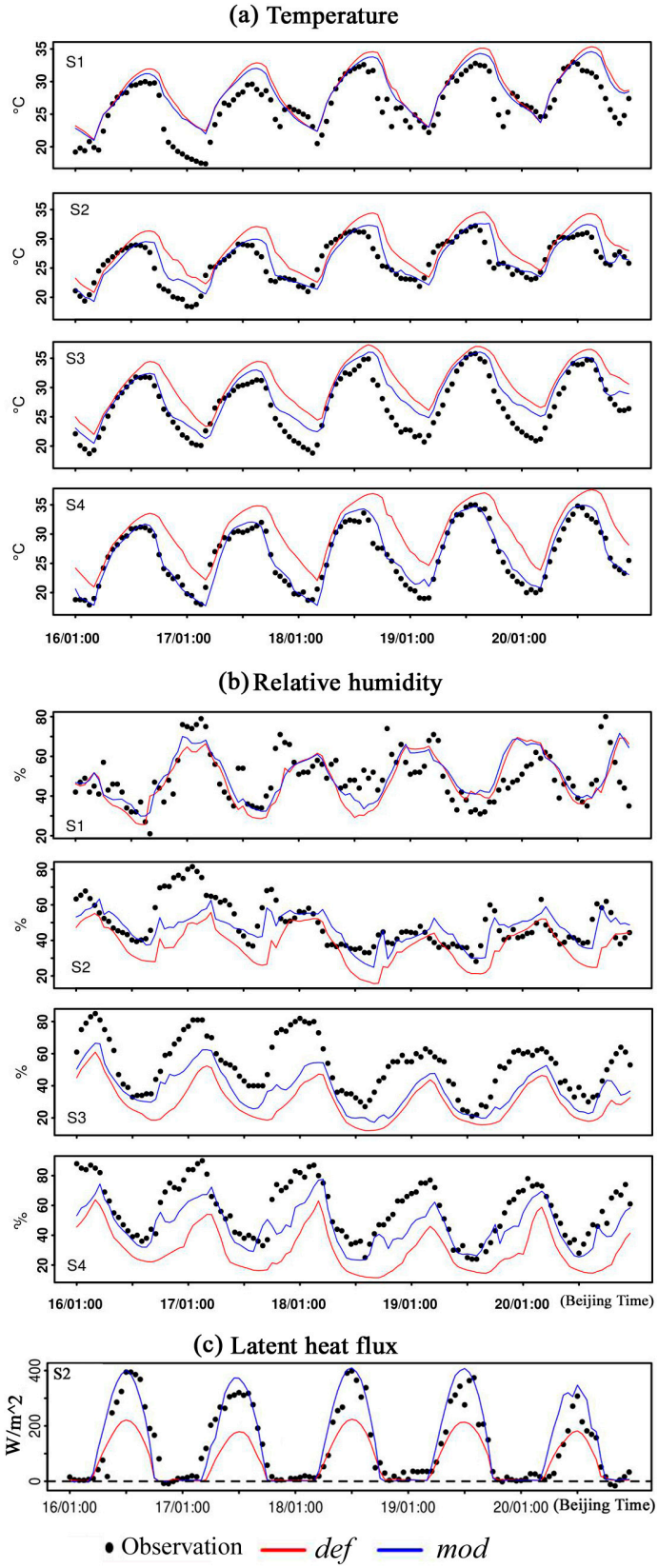

Figure 3. Comparisons of the observed and simulated (**a**) 2-m air temperature (T2), (**b**) 2-m relative humidity (RH) and (**c**) latent heat flux (LE) at the four stations (S1, S2, S3 and S4) during 16 July to 20 July.

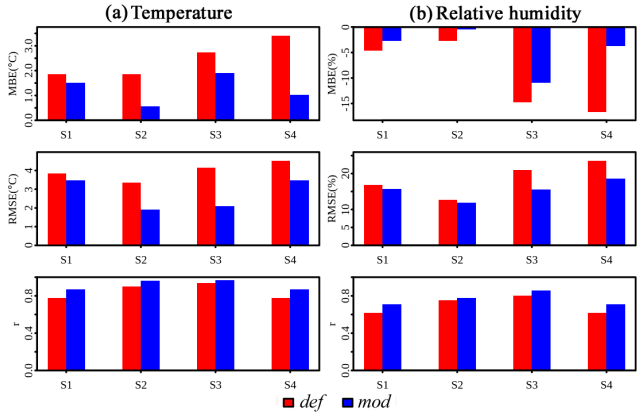

Figure 4. The mean bias error (MBE), root mean squared error (RMSE) and Pearson correlation coefficient (r) between the simulated and observed (**a**) air temperature and (**b**) relative humidity at 2 m at the four stations (S1, S2, S3 and S4).

A comparison of observed and simulated 10-m horizontal wind at the four meteorological stations, as represented by the *mod* and *def* simulations, is shown in Figure 5. Stations S1 and S2 are located in the upper part of oasis near its southern border and stations S3 and S4 are located in the lower part of the oasis near its northern border. Most of the simulated wind speeds (W_S) values are slightly higher than the observed values; 60 percent of the simulated W_S values lie within a range of 2–5 m/s, whereas the observed values range from 2 to 4 m/s. The reason for this bias in Ws is that the uncertainty of randomized turbulence processes hinders the accurate simulation of wind [65]. However, the trend in wind directions (W_D) agrees well with the observations. The observed dominant W_D is WNW or NW during daytime and WSW or SW at night for all four stations. The simulated W_D shows direction and diurnal changes that are consistent with the observations. This validation demonstrates that the simulated W_D agrees well with the observation and represents the circulation characteristics of the mountain-valley wind in the study area.

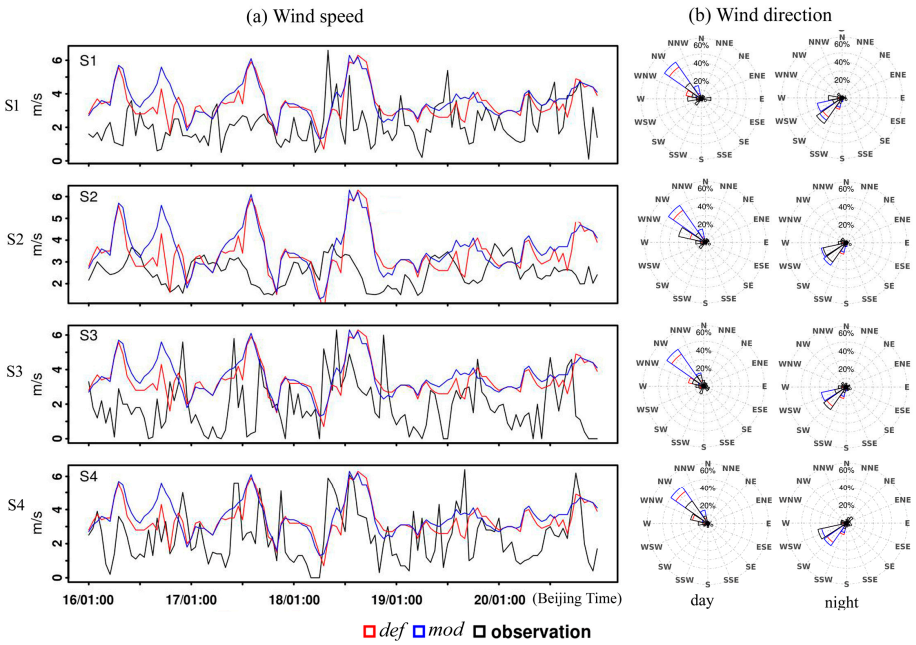

Figure 5. Comparison between the observed and simulated (**a**) wind speed (W_S) and (**b**) wind direction (W_D) from the *mod* and *def* simulations at the four stations (S1, S2, S3 and S4) during 16 July to 20 July.

3.3. Impacts of Mountains on Oases Effects in MODS

3.3.1. Spatial Patterns of Air Temperature

The 2-m air temperatures from both the *mod* and *non-oasis* simulations generally exhibit continuous stripe-like increases from the mountainous areas to the oasis areas and to the desert areas (Figure 6a–d). This pattern indicates that the spatial temperature pattern seen in the MODS reflects the lapse rate of temperature due to the elevation gradient difference within the MODS. An obvious temperature gradient line is observed along the northern boundary of the oasis in the *mod* simulation (Figure 6a,b) but not in the *non-oasis* simulation (Figure 6c,d), indicating that the water and heat differences between the oasis and desert areas obviously disturb the stripe-like increases in temperature in the MODS.

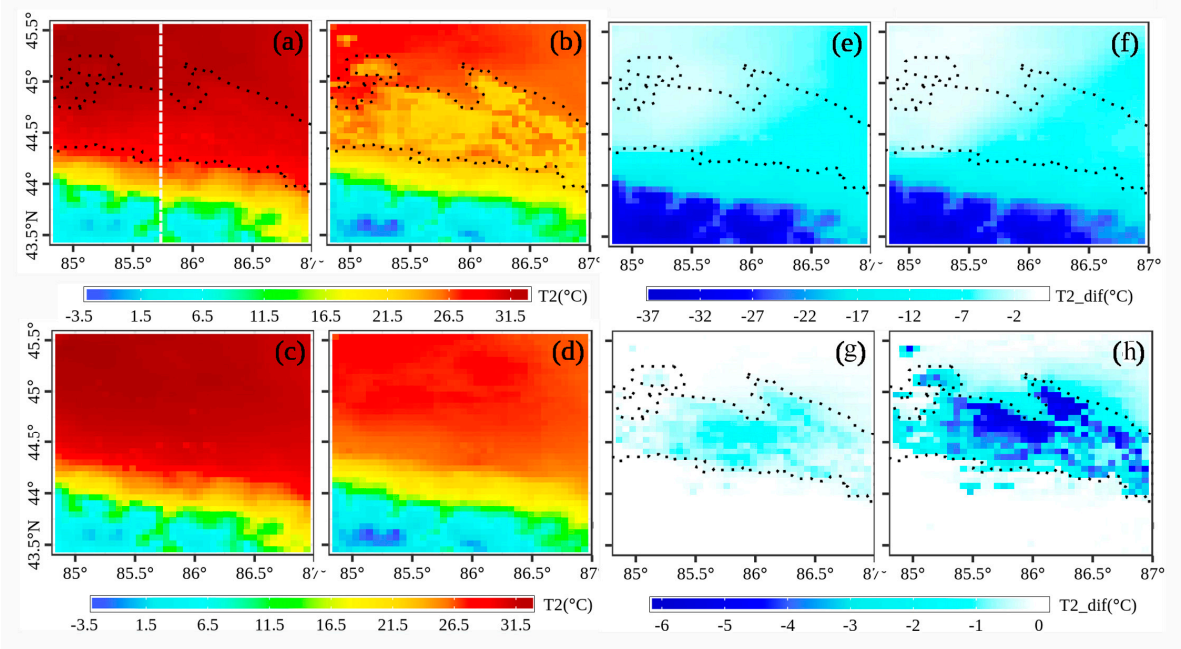

Figure 6. Mean 2-m air temperatures (T2) from the (**a**,**b**) *mod* simulation and (**c**,**d**) the *non-oasis* simulation; (**e**,**f**) and the differences between the *mod* simulation and *non-mountain* simulation; and (**g**,**h**) the differences between the *mod* simulation and the *non-oasis* simulation during daytime and nighttime, respectively. The black dotted line represents the border of the oasis and the white dotted line (**a**) represents the location of the vertical section (longitude 85.7° E) represented in Figure 7.

The mean near-surface air temperatures over the oasis area are 30.44 °C and 23.36 °C during the daytime and nighttime, respectively (Table 3). In contrast, the near-surface air temperatures over the desert are approximately 32.5 °C and 28.0 °C, respectively (Figure 6a,b). The differences in the near-surface air temperatures between the oasis and desert areas indeed indicate that the oasis areas represent a "cold island" compared to the surrounding desert during daytime and nighttime. The intensity of this "cold island" resulting from the oasis cooling effect is as large as −0.61 °C in daytime and as large as −3.37 °C at night, as computed using the mean oasis temperature difference between the *mod* simulation and *non-oasis* simulation (these differences are statistically significant at $p < 0.01$, Table 3). During the daytime, because the soil moisture and thermal capacity values are higher in the oasis areas than the desert areas, more energy is required to increase the temperatures over the oasis areas and evapotranspiration takes place in the oasis, causing cooling [28] (as can be seen in Figure S5a,c). The possible reasons for the more intense cooling effect of the oasis at night include evaporation from the surface soil (Figure S4f) and the lapse rate of temperature; the slightly higher elevation of the oasis areas (Figure 6e,f) enhances the intensity of this "cold island" effect. Note that the near-surface temperature patterns from the *non-mountain* simulation (Figure S1a,b) and the difference

patterns between the *mod* simulation and the *non-mountain* simulation (Figure 6e,f) are also consistent with circulation patterns, illustrating that the water and heat patterns in the study area are controlled by larger-scale circulation and the climate background in the absence of high-relief terrain.

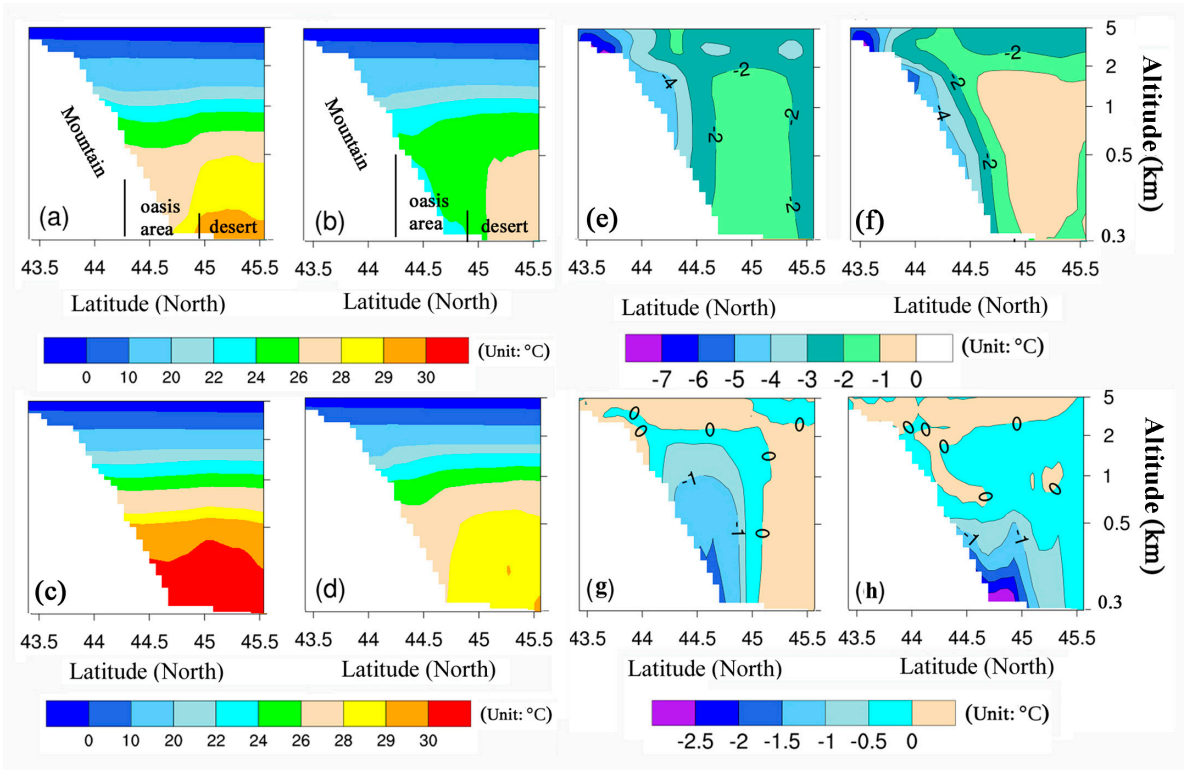

Figure 7. The same as Figure 6 but showing for a vertical cross section of air temperature along the white line shown in Figure 6a.

Table 3. Statistical significance of the differences in temperature and humidity between the *mod* and *non-oasis* simulations, as assessed using Student's *t*-test.

Time Periods	Statistics	Temperature (°C)		Specific Humidity (g kg^{-1})	
		mod	*non-oasis*	*mod*	*non-oasis*
Day	Mean	30.44	31.05	9.99	8.43
	Variance	1.67	1.69	0.78	0.38
	p-value	3.16×10^{-10} << 0.01 *		1.64×10^{-113} << 0.01 *	
Night	Mean	23.36	26.73	10.05	9.97
	Variance	1.77	1.50	0.38	0.47
	p-value	8.47×10^{-165} << 0.01 *		0.075 > 0.05	

* Indicates that the difference between the mod and the non-oasis simulations is extremely significant.

The continuous stripe-like temperature patterns and the oasis cooling effect are further illustrated by the vertical section of temperature patterns from the *mod* and *non-oasis* simulations and the temperature differences between the *mod* and the *non-oasis* simulations and between the *mod* and *non-mountain* simulations (Figure 7). In the daytime, the air temperatures in the oasis area in the *mod* simulation are clearly lower than those over the northern desert area and the southern mountainous area at the same altitude of approximately 1500 m and this temperature pattern forms a concave-shaped vertical temperature pattern in the MODS (Figure 7a). At night, a clearly defined temperature inversion layer (TIL) is observed near the surface over the oasis area. Its thickness varies from 200 m in the southern part of the oasis with an elevation of 450 m to 600 m in the northern part with an elevation of

300 m (Figure 7b). However, the concave-shaped vertical temperature pattern observed during the daytime and the TIL that developed during the nighttime are not observed in the *non-oasis* simulation (Figure 7c,d), indicating the concave low-temperature center and the TIL over the oasis areas result from the oasis cooling effect. Based on the differences between the *mod* and *non-oasis* simulations, the "cold island" effect of the oasis extends to a height of approximately 1.5 km above the oasis surface, as shown by the n-shaped cooling center (Figure 7d,g). Moreover, the cooling effect of the oasis extends horizontally into the desert-oasis transition areas to a distance of approximately 25 km (Figures 6h and 7h) at night due to the mountain-wind. In addition, the existence of high-relief terrain (mountains) decreases the whole temperature pattern over the basin during the daytime and the nighttime, based on the differences between the *non-oasis* and *non-mountain* simulations (Figures 6 and 7e,f).

3.3.2. Spatial Patterns of Humidity

The mean near-surface specific humidity (Q2) values over the oasis in the *mod* simulation are 9.99 g kg^{-1} and 10.05 g kg^{-1} during the daytime and nighttime, respectively (Table 3). In contrast, values of approximately 8.4 g kg^{-1} (Figure 8a) and 9.9 g kg^{-1} (Figure 8b) occur at almost the same elevation in the surrounding desert areas, respectively. The oasis indeed represents a "wet island" compared with the surrounding desert at almost the same elevation but the mechanism underlying the "wet island" effect differs between daytime and nighttime.

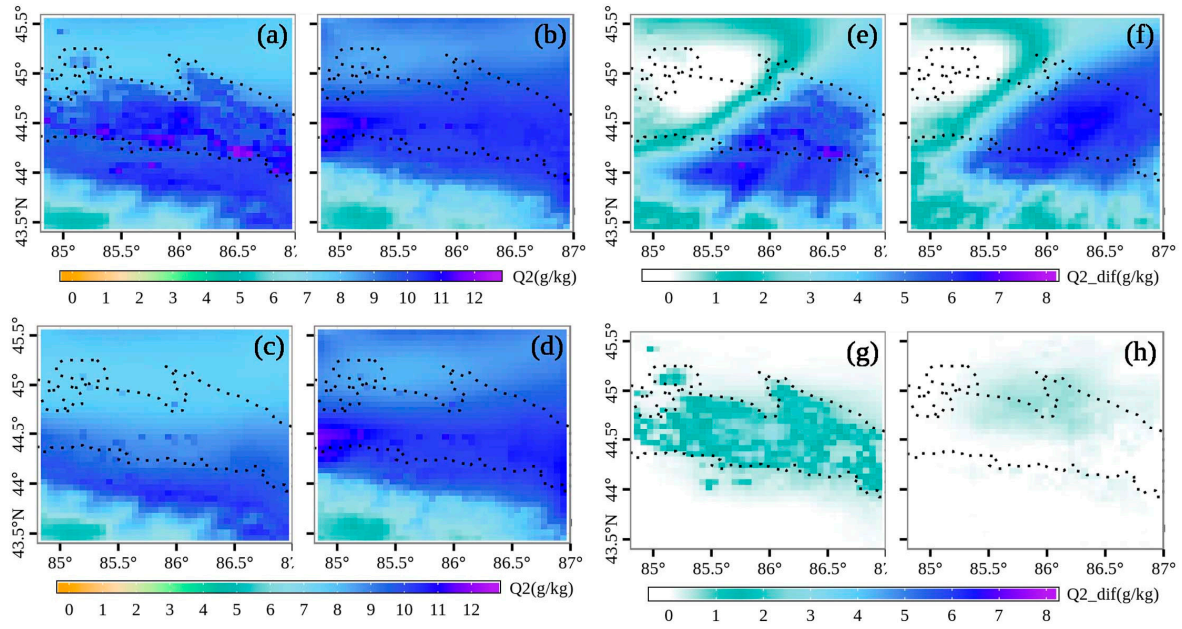

Figure 8. The same as Figure 6 but for surface specific humidity Q2 (g kg^{-1}).

A clearly defined humidity gradient line along the northern boundary of the oasis during the daytime is observed in the *mod* simulation (Figure 8a) but the gradient line is not observed at night in the *mod* simulation (Figure 8b) or in the *non-oasis* simulation (Figure 8c,d). The patterns of differences between the *mod* and the *non-oasis* simulations show that there is indeed a remarkable difference in specific humidity over the oasis areas during the daytime, whereas a slight difference occurs along the northern oasis boundary and in the desert area at night (Figure 8g,h). Based on Student's *t*-test, the mean humidity difference over the oasis between the *mod* simulation and the *non-oasis* simulation is extremely statistically significant (the *p*-value is far less than 0.01) during the daytime but statistically insignificant (the *p*-value is 0.075) at night (Table 3). This result indicates that the "wet island" results from the wetting effect of the oasis during the daytime but the cause during the nighttime is uncertain. The mean intensity of this "wet island" resulting from the oasis wetting effect is 1.56 g kg^{-1} during

the daytime (Table 3). In addition, nighttime moisture differences between the *mod* and the *non-oasis* simulations are mainly located along the northern boundary of the oasis area, rather than over the oasis itself (Figure 7h). This result appears to be consistent with the circulation patterns, suggesting that the wetting effect of the oasis might be present at night but that the spatial extent of the wetting effect changes due to the mountain wind. Moreover, the surface specific humidity patterns from the *non-mountain* simulation (Figure S2a,b) and the differences between the *mod* and the *non-mountain* simulations (Figure 8e,f) are also consistent with the circulation patterns. Thus, the water and heat patterns in the study area would be controlled by larger-scale circulation patterns and the climate background in the absence of high-relief terrain.

Figure 9 shows the vertical section of humidity patterns from the *mod* and *non-oasis* simulations, as well as the differences between the *mod* and *non-oasis* simulations and between the *mod* and *non-mountain* simulations. The specific humidity in the mountainous area at an equivalent altitude of 1 km during the daytime and nighttime is higher than that over the basin area at the same elevation of 1 km in the *non-oasis* simulation (Figure 9c,d). This higher specific humidity in the mountainous areas may be due to the wetting effect of daytime evaporation from forest and grassland and the radiative cooling of mountainous areas decreases the saturated vapor pressure, leading to a higher specific humidity [66] during nighttime.

The differences between the *mod* and *non-oasis* simulations (Figure 9g,h) and between the *mod* and *non-mountain* simulations (Figure 9e,f) provide further confirmation of the wetting effects of oases and mountains based on the decrease in the cooling gradient from the oasis surface over a distance of approximately 1 km (Figure 9g,h) and from the mountainous areas to their surroundings (Figure 9e,f). Moreover, the wetting effect of the oasis areas at night extends horizontally into the desert areas to a distance of approximately 25 km (Figures 8h and 9h). This horizontal extension results primarily from the ground-hugging nighttime mountain wind, since the extension is consistent with the direction of the mountain wind (Figure 10b,d).

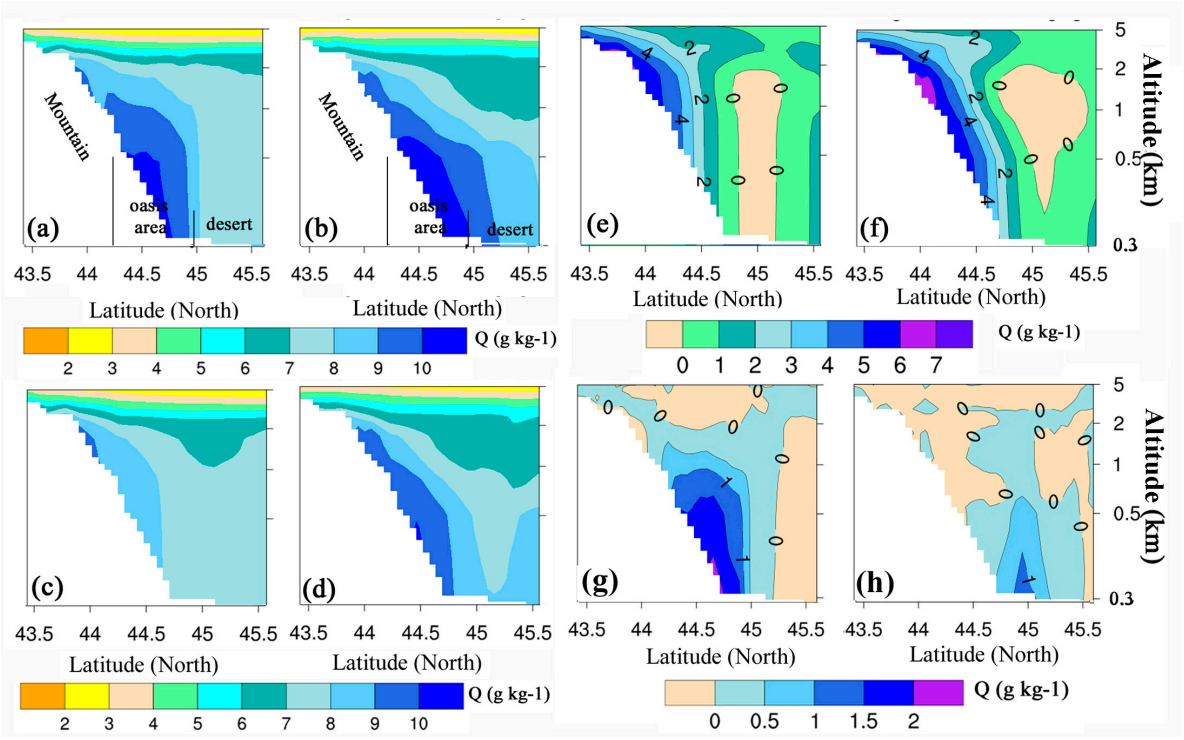

Figure 9. Same as Figure 6 but for the vertical section of specific humidity Q (g kg^{-1}) along the white line (longitude 85.7° E) shown in Figure 6a.

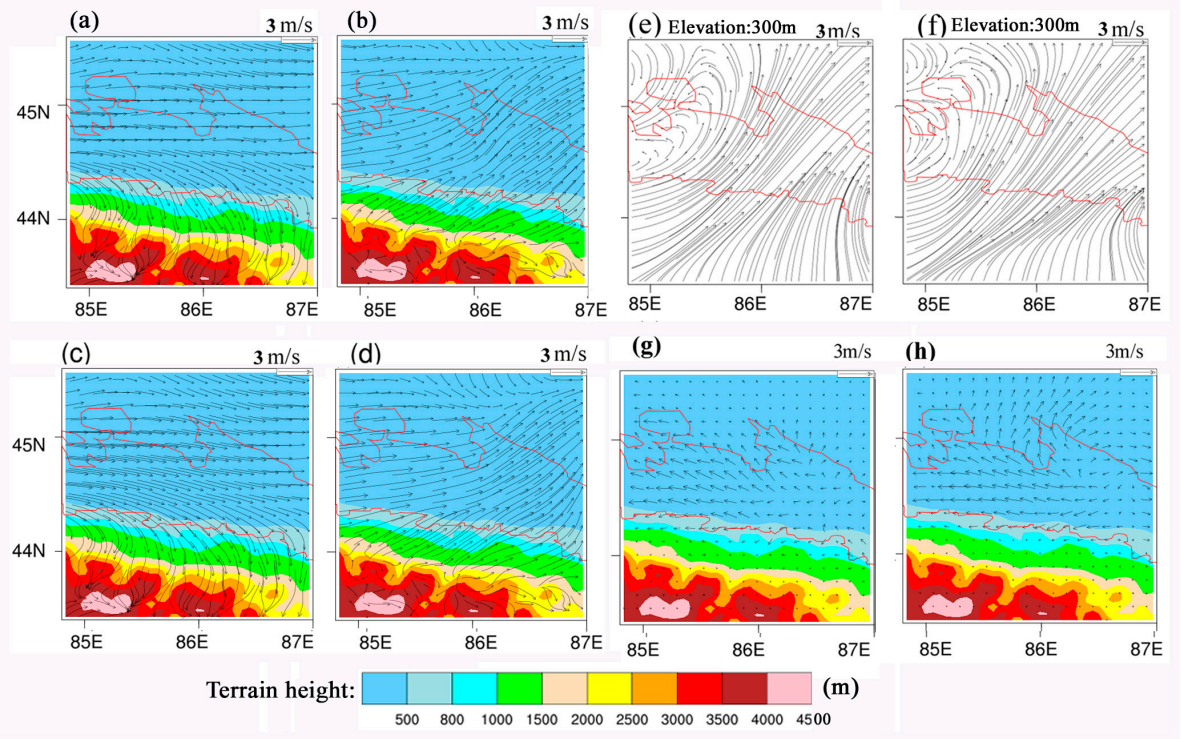

Figure 10. The mean diurnal W_S and W_D patterns (mean wind speed and direction at a height of 10 m during the daytime and nighttime) in the *mod*, *non-oasis* and *non-mountain* simulations and the differences between the *mod* and *non-oasis* simulations. (**a**) Daytime Ws and W_D from the *mod* simulation; (**b**) nighttime Ws and W_D from the *mod* simulation; (**c**) daytime Ws and W_D from the *non-oasis* simulation; (**d**) nighttime Ws and W_D from the *non-oasis* simulation; (**e**) daytime Ws and W_D from the *non-mountain* simulation; (**f**) nighttime Ws and W_D from the *non-mountain* simulation; (**g**) daytime Ws and W_D difference between the *mod* and *non-oasis* simulations; (**h**) nighttime Ws and W_D difference between the *mod* and *non-oasis* simulations. The red line represents the border of the oasis.

3.3.3. Spatial Patterns of the 10-m Horizontal Circulation

Figure 10 shows the diurnal mean W_S and W_D patterns from the *mod, non-oasis and non-mountain* simulations, as well as the differences between the *mod* and *non-oasis* simulations. In the context of the prevailing westerly wind, a wind direction of WNW with a wind speed of approximately 3 m/s occurs during the daytime (Figure 10a,c), whereas a wind direction of SW with a wind speed of approximately 4 m/s occurs at night (Figure 9b,d), as observed in both the *mod* and *non-oasis* simulations covering the MODS. An intense southwesterly wind with a wind speed exceeding 7 m/s is observed during both daytime and nighttime in the *non-mountain* simulation (Figure 10e,f) and the intense southwesterly wind represents a combination of the prevailing westerly wind and the summer subtropical jet stream resulting from the Southwest Asian low-pressure system over northeastern India [39,67]. However, the intense southwesterly wind is blocked in the *mod* and *non-oasis* simulations. Therefore, the diurnal change in the wind direction from WNW to SW in the *mod* and *non-oasis* simulations is produced by the high-relief terrain, further demonstrating the existence of mountain-valley winds in the MODS.

The difference between the *mod* simulation and the *non-oasis* simulation is characterized by an obvious divergent wind blowing from the center of the oasis area to the surrounding desert with a speed of less than approximately 1.5 m/s at a height of 10 m height (Figure 10g,h). This divergent wind is oriented in the opposite direction of the combination of the mountain-valley wind and the prevailing westerly wind. However, no obvious downdrafts or updrafts occur over the oasis or deserts

based on the vertical component difference between the *mod* and *non-oasis* simulations (Figure S3). This divergence indicates that OBC may indeed exist between the oasis and desert areas and the possible OBC is counteracted by the stronger background circulation produced by the combination of the mountain-valley wind and the prevailing westerly wind.

4. Comparison with Previous Studies and an Assessment of Model Uncertainties

In this study, the effects of oases on temperature, humidity and regional circulation patterns within an arid MODS in the NTM were investigated using the WRF model with actual LC, albedo, LAI and GVF datasets. The *mod* simulation provides a significantly better representation of diurnal temperature and humidity due to use of updated datasets and better reflects the exchanges of water and heat in the MODS.

The differences between the *mod* and *non-oasis* simulations show the typical "cold island" effect and "wet island" effect of an oasis during the day. Thus, a TIL develops over the oasis areas at night from the *mod* simulation. The oasis cooling-wetting effect reaches a vertical height of approximately 1.5 km above the oasis surface and this result is similar to findings reported in previous investigations [6,17,21,24,26–28]. However, our study also contributes certain new findings. The Tianshan Mountains act as the background of the oasis-desert interaction and exert a cooling and wetting effect on the whole MODS in the NTM region, as evidenced by the differences between the *mod* and the *non-mountain* simulations. Moreover, the horizontal range of the oasis wetting effect appears to extend into the desert areas, rather than being restricted over the oasis areas, due to the presence of the mountain wind at night. This horizontal extension may produce favorable conditions for desert plants in the oasis-desert transition zone.

In previous studies, researchers proposed the concept that oases have a self-supporting mechanism originating from OBC. They argued that the OBC between an oasis and the surrounding desert helps maintain the ecological stability of the oasis by reducing heat and moisture exchange [21,24,26,28]. The results from the *mod* simulation and the differences between *the mod* and *non-oasis* simulations show that the water and heat differences between the oasis and surrounding desert do produce OBC (Figure 10e,f). However, OBC is not observed in the actual weather or climate conditions (the *mod* simulation in this study) (Figure 10a,b) because it is counteracted by the stronger background circulation that results from a combination of mountain-valley wind and the prevailing westerly wind in the MODS. Therefore, the effects of OBC on the ecological stability of oasis systems within an MODS may have been overestimated by previous studies. Consequently, studies related to oasis effects should consider the regional context of the MODS, if the oasis is located in a large mountain-basin system. Such investigations will help provide a better understanding of the ecological and climatic effects of oasis systems but also may result in the identification of new features of such systems. In addition, this study represents necessary preliminary work for further investigating the contributions of oasis expansion to historical and future climate changes at local or regional scales. Whether and how the typical wetting and cooling effects of oases impact local or regional climate change will be further investigated in the next stage of this work, which will include long-period simulations.

Some limitations in the modeling must be examined in future studies. For example, we found that the simulated temperatures were generally somewhat overestimated and that the relative humidity was slightly underestimated. These errors may be attributed to the evaporation from soils resulting from occasional irrigation. This process was not considered in the simulations [6,28] because the WRF model describes irrigation and irrigated areas in terms of different biophysical parameters between irrigated cropland and rain-fed cropland, instead of using a physical or mechanistic description of irrigation. An irrigation scheme will be added and a sensitivity analysis will be carried out in the future work to determine whether this bias can be corrected.

5. Conclusions

In this study, the effects of oasis areas were investigated within a complete MODS located in the NTM using the WRF model. Studies of oasis effects should consider the entire MODS, which will help to fully understand the ecological and climatic effects of oasis systems. The typical "cold-wet" island effects of the oasis, nighttime TIL over oasis areas and OBC are fully described within the context of the MODS in this study through the use of the WRF model with actual LC, albedo, LAI and GVF datasets. The Tianshan Mountains exert a cooling and wetting effects on the whole MODS in the NTM region. The mountain wind causes the "cold-wet" island effects of the oasis to extend into the surrounding desert area at night, which may produce conditions favorable for desert plants in the oasis-desert transition zone. However, the OBC was counteracted by stronger background winds resulting from a combination of the prevailing westerly winds and the mountain-valley wind in the MODS. The proposed self-supporting mechanism of the oasis associated with the OBC cannot play a significant role in maintaining the stability of the oasis in this MODS.

Supplementary Materials: The following are available online at www.mdpi.com/2073-4433/8/11/212/s1.

Acknowledgments: This work was supported financially by the International Partnership Program of the Chinese Academy of Science (Grant No. 131965KYSB20160004) and the National Natural Science Foundation of China (Grant Nos. U1303382 and 41671108). The authors declare no conflict of interest. All of the datasets will be available from XIEG for 5 years, including the data used to generate the figures, the actual LC, albedo, LAI and GVF datasets used in WRF and the original WRF outputs used in this paper.

Author Contributions: Miao Zhang, Geping Luo and Rafiq Hamdi conceived and designed the experiments; Miao Zhang, Yuan Qiu and Xinxin Wang performed the experiments and analyzed the data; and Miao Zhang, Philippe De Maeyer, Rafiq Hamdi and Alishir Kurban jointly revised the paper.

Conflicts of Interest: The authors declare no conflict of interest.

Abbreviations

The following abbreviations are used in this manuscript:

AVHRR	Advanced Very High Resolution Radiometer
BRDF	Bidirectional reflectance distribution function
CA	Central Asia
LAI	Leaf area index
LE	Latent heat flux
LC	Land cover
MBE	Mean bias error
MM5	Fifth-generation Penn State/NCAR Mesoscale Model
MODIS	MODerate Resolution Imaging Spectroradiometer
MODS	Mountain-oasis-desert System
NCAR	National Center for Atmospheric Research
NCEP	National Centers for Environmental Prediction
NTM	North Tianshan Mountains
OBC	Oasis breeze circulation
Q2	Specific humidity at 2 m
r	Pearson correlation coefficient
RMSE	Root mean squared error
RH	2-m relative humidity
T2	2-m air temperature
TIL	Temperature inversion layer
USGS	U.S. Geological Survey
GVF	Green vegetation fraction
WRF	Weather Research and Forecasting model
WS	Wind speed
WD	Wind direction

Appendix A

WRFv 3.6.1 is available from http://www2.mmm.ucar.edu/wrf/users/downloads.html and the MODIS datasets can be obtained from https://modis.gsfc.nasa.gov/data. All of the other code and datasets are available from https://zenodo.org/deposit/new, including the data, the code used to generate figures, the actual LC, albedo, LAI and GVF datasets used in this study and the original WRF output in the paper.

References

1. Souza, V.; Espinosa-Asuar, L.; Escalante, A.E.; Eguiarte, L.E.; Farmer, J.; Forney, L.; Lloret, L.; Rodríguez-Martínez, J.M.; Soberón, X.; Dirzo, R. An Endangered Oasis of Aquatic Microbial Biodiversity in the Chihuahuan Desert. *Proc. Natl. Acad. Sci. USA* **2006**, *103*, 6565–6570. [CrossRef] [PubMed]
2. Smith, J.R.; Hawkins, A.L.; Asmerom, Y.; Polyak, V.; Giegengack, R. New Age Constraints on the Middle Stone Age Occupations of Kharga Oasis, Western Desert, Egypt. *J. Hum. Evol.* **2007**, *52*, 690–701. [CrossRef] [PubMed]
3. Soltan, M. Evaluation of Ground Water Quality in Dakhla Oasis (Egyptian Western Desert). *Environ. Monit. Assess.* **1999**, *57*, 157–168. [CrossRef]
4. Li, J.; Zhao, C.; Zhu, H.; Li, Y.; Wang, F. Effect of plant species on shrub fertile island at an oasis–desert ecotone in the south junggar basin, china. *J. Arid Environ.* **2007**, *71*, 350–361. [CrossRef]
5. Luo, G.P.; Feng, Y.X.; Zhang, B.P.; Cheng, W.M. Sustainable Land-Use Patterns for Arid Lands: A Case Study in the Northern Slope Areas of the Tianshan Mountains. *J. Geogr. Sci.* **2010**, *20*, 510–524. [CrossRef]
6. Meng, X.H.; Lü, S.H.; Zhang, T.T.; Guo, J.X.; Gao, Y.H.; Bao, Y.; Wen, L.J.; Luo, S.Q.; Liu, Y.P. Zy-Numerical Simulations of the Atmospheric and Land Conditions over the Jinta Oasis in Northwestern China with Satellite-Derived Land Surface Parameters. *Int. J. Climatol.* **2009**, *114*. [CrossRef]
7. Zhang, H.; Wu, J.-W.; Zheng, Q.-H.; Yu, Y.-J. A Preliminary Study of Oasis Evolution in the Tarim Basin, Xinjiang, China. *J. Arid Environ.* **2003**, *55*, 545–553.
8. Zhang, Q.; Luo, G.; Li, L.; Zhang, M.; Lv, N.; Wang, X. An Analysis of Oasis Evolution Based on Land Use and Land Cover Change: A Case Study in the Sangong River Basin on the Northern Slope of the Tianshan Mountains. *J. Geogr. Sci.* **2017**, *27*, 223–239. [CrossRef]
9. Jia, B.; Zhang, Z.; Ci, L.; Ren, Y.; Pan, B.; Zhang, Z. Oasis Land-Use Dynamics and Its Influence on the Oasis Environment in Xinjiang, China. *J. Arid Environ.* **2004**, *56*, 11–26. [CrossRef]
10. Sun, D.; Zhao, C.; Wei, H.; Peng, D. Simulation of the Relationship between Land Use and Groundwater Level in Tailan River Basin, Xinjiang, China. *Quat. Int.* **2011**, *244*, 254–263. [CrossRef]
11. Wang, Y.; Xiao, D.; Li, Y.; Li, X. Soil Salinity Evolution and Its Relationship with Dynamics of Groundwater in the Oasis of Inland River Basins: Case Study from the Fubei Region of Xinjiang Province, China. *Environ. Monit. Assess.* **2008**, *140*, 291–302. [CrossRef] [PubMed]
12. Li, X.; Cheng, G.D.; Liu, S.M.; Xiao, Q.; Ma, M.G.; Jin, R.; Che, T.; Liu, Q.H.; Wang, W.Z.; Qi, Y. Heihe Watershed Allied Telemetry Experimental Research (Hiwater): Scientific Objectives and Experimental Design. *Bull. Am. Meteor. Soc.* **2013**, *94*, 1145–1160. [CrossRef]
13. Li, X.W.; Jin, M.G.; Zhou, N.Q.; Huang, J.; Jiang, S.; Telesphore, H. Evaluation of Evapotranspiration and Deep Percolation Under Mulched Drip Irrigation in an Oasis of Tarim Basin, China. *J. Hydrol.* **2016**, *538*, 677–688. [CrossRef]
14. Ling, H.B.; Xu, H.L.; Fu, J.Y.; Fan, Z.L.; Xu, X.W. Suitable Oasis Scale in a Typical Continental River Basin in an Arid Region of China: A Case Study of the Manas River Basin. *Quat. Int.* **2013**, *286*, 116–125. [CrossRef]
15. Wang, P.; Li, X.Y.; Huang, Y.M.; Liu, S.M.; Xu, Z.W.; Wu, X.C.; Ma, Y.J. Numerical Modeling the Isotopic Composition of Evapotranspiration in an Arid Artificial Oasis Cropland Ecosystem with High-Frequency Water Vapor Isotope Measurement. *Agric. For. Meteorol.* **2016**, *230*, 79–88. [CrossRef]
16. Li, X.; Yang, K.; Zhou, Y. Progress in the Study of Oasis-Desert Interactions. *Agric. For. Meteorol.* **2016**, *230*, 1–7. [CrossRef]
17. Liu, S.H.; Liu, H.P.; Hu, Y.; Zhang, C.Y.; Liang, F.M.; Wang, J.H. Numerical Simulations of Land Surface Physical Processes and Land-Atmosphere Interactions over Oasis-Desert/Gobi Region. *Sci. China Ser. D Earth Sci.* **2007**, *50*, 290–295. [CrossRef]
18. Su, C.X.; Hu, Y.Q. The Structure of the Oasis Cold Island in the Planetary Boundary Layer. *Acta Meteorol. Sin.* **1987**, *45*, 322–328.

19. Rosenberg, N.J. Seasonal Patterns in Evapotranspiration by Irrigated Alfalfa in the Central Great Plains. *Agron. J.* **1969**, *61*, 879–886. [CrossRef]
20. Wang, J.; Sahashi, K.; Ohtaki, E.; Maitani, T.; Tsukamoto, O.; Mistsuta, Y.; Kobayashi, T.; Zhang, H.; Li, Q.; Xie, Z. Energy and Mass Transfer Characteristics of Soil-Vegetationatmosphere System in Oasis Area-Outline of the Bio Meteorological Observation Period (Bop). In Proceedings of the International Symposium on HEIFE, Kyoto University, Kyoto, Japan, 8–11 November 1993; pp. 507–514.
21. Chu, P.; Liv, S.H.; Chen, Y.C. A Numerical Modeling Study on Desert Oasis Self-Supporting Mechanisms. *J. Hydrol.* **2005**, *312*, 256–276. [CrossRef]
22. Gao, Y.H.; Chen, Y.C.; Lv, S.H. Numerical Simulation of the Critical Scale of Oasis Maintenance and Development in the Arid Regions of Northwest China. *Adv. Atmos. Sci.* **2004**, *21*, 113–124. [CrossRef]
23. Han, B.; Lv, S.; Ao, Y. Analysis on the Interaction between Turbulence and Secondary Circulation of the Surface Layer at Jinta Oasis in Summer. *Adv. Atmos. Sci.* **2010**, *27*, 605. [CrossRef]
24. Lv, S.H.; Shang, L.Y.; Liang, L.; Luo, S.Q. Numerical Simulation of Microclimate Effect in Jinta Oasis. *Plateau Meteorol.* **2005**, *24*, 649–655.
25. Meng, X.; Lu, S.; Gao, Y.; Guo, J. Simulated Effects of Soil Moisture on Oasis Self-Maintenance in a Surrounding Desert Environment in Northwest China. *Int. J. Climatol.* **2015**, *35*, 4116–4125. [CrossRef]
26. Meng, X.H.; Lu, S.; Zhang, T.; Ao, Y.; Li, S.; Bao, Y.; Wen, L.; Luo, S. Impacts of Inhomogeneous Landscapes in Oasis Interior on the Oasis Self-Maintenance Mechanism by Integrating Numerical Model with Satellite Data. *Hydrol. Earth Syst. Sci.* **2012**, *16*, 3729–3738. [CrossRef]
27. Nnamchi, H.C. Numerical Simulation of Fluxes Generated by Inhomogeneities of the Underlying Surface over the Jinta Oasis in Northwestern China. *Adv. Atmos. Sci.* **2011**, *28*, 887–906.
28. Wen, X.H.; Lu, S.H.; Jin, J.M. Integrating Remote Sensing Data With Wrf for Improved Simulations of Oasis Effects on Local Weather Processes Over an Arid Region in Northwestern China. *J. Hydrol.* **2012**, *13*, 573–587. [CrossRef]
29. Zardi, D.; Whiteman, C.D. Diurnal Mountain Wind Systems. *Bull. Am. Meteorol. Soc.* **2013**, 35–119. [CrossRef]
30. Helgason, W.; Pomeroy, J.W. Characteristics of the Near-Surface Boundary Layer within a Mountain Valley During Winter. *J. Appl. Meteorol.* **2012**, *51*, 583–597. [CrossRef]
31. Yan, J.W.; Liu, J.Y.; Chen, B.Z.; Feng, M.; Fang, S.F.; Xu, G.; Zhang, H.F.; Che, M.L.; Liang, W.; Hu, Y.F. Changes in the Land Surface Energy Budget in Eastern China over the Past Three Decades: Contributions of Land-Cover Change and Climate Change. *J. Clim.* **2014**, *27*, 9233–9252. [CrossRef]
32. Lenderink, G.; Van Ulden, A.; Van den Hurk, B.; Van Meijgaard, E. Summertime Inter-Annual Temperature Variability in an Ensemble of Regional Model Simulations: Analysis of the Surface Energy Budget. *Clim. Chang.* **2007**, *81*, 233–247. [CrossRef]
33. Vidale, P.L.; Lüthi, D.; Wegmann, R.; Schär, C. European Summer Climate Variability in a Heterogeneous Multi-Model Ensemble. *Clim. Chang.* **2007**, *81*, 209–232. [CrossRef]
34. Müller, O.V.; Berbery, E.H.; Alcaraz-Segura, D.; Ek, M.B. Regional Model Simulations of the 2008 Drought in Southern South America Using a Consistent Set of Land Surface Properties. *J. Clim.* **2014**, *27*, 6754–6778. [CrossRef]
35. Cowan, P.J. Geographic Usage of the Terms Middle Asia and Central Asia. *J. Arid Environ.* **2007**, *69*, 359–363. [CrossRef]
36. Li, C.F.; Zhang, C.; Luo, G.P.; Chen, X.; Maisupova, B.; Madaminov, A.A.; Han, Q.F.; Djenbaev, B.M. Carbon Stock and Its Responses to Climate Change in Central Asia. *Glob. Chang. Biol.* **2015**, *21*, 1951–1967. [CrossRef] [PubMed]
37. Bothe, O.; Fraedrich, K.; Zhu, X.H. Precipitation Climate of Central Asia and the Large-Scale Atmospheric Circulation. *Theor. Appl. Climatol.* **2012**, *108*, 345–354. [CrossRef]
38. Sorg, A.; Bolch, T.; Stoffel, M.; Solomina, O.; Beniston, M. Climate Change Impacts on Glaciers and Runoff in Tien Shan (Central Asia). *Nat. Clim. Chang.* **2012**, *2*, 725–731. [CrossRef]
39. Lioubimtseva, E.; Cole, R.; Adams, J.M.; Kapustin, G. Impacts of Climate and Land-Cover Changes in Arid Lands of Central Asia. *J. Arid Environ.* **2005**, *62*, 285–308. [CrossRef]
40. Yao, Y.H.; Zhang, B.P. A Preliminary Study of the Heating Effect of the Tibetan Plateau. *PLoS ONE* **2013**, *8*, e68750. [CrossRef] [PubMed]
41. Skamarock, W.C.; Klemp, J.B.; Dudhia, J.; Gill, D.O.; Barker, D.M.; Wang, W.; Powers, J.G. *A Description of the Advanced Research Wrf*; Version 2; DTIC Document: Fort Belvoir, VA, USA, 2005.

42. Yin, J.F.; Zhan, X.W.; Zheng, Y.F.; Hain, C.R.; Ek, M.; Wen, J.; Fang, L.; Liu, J.C. Improving Noah Land Surface Model Performance Using Near Real Time Surface Albedo and Green Vegetation Fraction. *Agric. For. Meteorol.* **2016**, *218*, 171–183. [CrossRef]
43. Tewari, M.; Chen, F.; Wang, W.; Dudhia, J.; LeMone, M.A.; Mitchell, K.; Ek, M.; Gayno, G.; Wegiel, J.; Cuenca, R.H. Implementation and verification of the unified noah land surface model in the WRF model. In Proceedings of the 20th Conference on Weather Analysis and Forecasting/16th Conference on Numerical Weather Prediction, Seattle, WA, USA, 10–15 January 2004; pp. 11–15.
44. Chen, F.; Mitchell, K.; Schaake, J.; Xue, Y.K.; Pan, H.L.; Koren, V.; Duan, Q.Y.; Ek, M.; Betts, A. Modeling of Land Surface Evaporation by Four Schemes and Comparison with Fife Observations. *Int. J. Climatol.* **1996**, *101*, 7251–7268. [CrossRef]
45. Seungbum, H.; Lakshmi, V.; Small, E.E.; Chen, F.; Tewari, M.; Manning, K.W. Effects of Vegetation and Soil Moisture on the Simulated Land Surface Processes from the Coupled WRF/Noah Model. *Int. J. Climatol.* **2009**, *114*.
46. Branch, O.; Warrach-Sagi, K.; Wulfmeyer, V.; Cohen, S. Simulation of Semi-Arid Biomass Plantations and Irrigation Using the WRF-Noah Model–a Comparison with Observations from Israel. *Hydrol. Earth Syst. Sci.* **2014**, *18*, 1761–1783. [CrossRef]
47. Chen, F.; Dudhia, J. Coupling an Advanced Land Surface-Hydrology Model with the Penn State-Ncar mm5 Modeling System. Part I: Model Implementation and Sensitivity. *Mon. Weather Rev.* **2001**, *129*, 569–585. [CrossRef]
48. Qiu, Y.; Hu, Q.; Zhang, C. WRF Simulation and Downscaling of Local Climate in Central Asia. *Int. J. Climatol.* **2017**, *37*, 513–528. [CrossRef]
49. Song, Y.H.; Noh, Y.; Dudhia, J. A New Vertical Diffusion Package with an Explicit Treatment of Entrainment Processes. *Mon. Weather Rev.* **2006**, *134*, 2318–2341.
50. Song, Y.H.; Dudhia, J.; Chen, S.H. A Revised Approach to Ice Microphysical Processes for the Bulk Parameterization of Clouds and Precipitation. *Mon. Weather Rev.* **2004**, *132*, 103–120.
51. Bretherton, C.S.; McCaa, J.R.; Grenier, H. A New Parameterization for Shallow Cumulus Convection and Its Application to Marine Subtropical Cloud-Topped Boundary Layers. Part i: Description and 1d Results. *Mon. Weather Rev.* **2004**, *132*, 864–882. [CrossRef]
52. Collins, W.; Rasch, P.; Boville, B.A.; Hack, J.J.; McCaa, J.R.; Williamson, D.L.; Kiehl, J.T.; Briegleb, B.; Bitz, C.; Lin, S.J. Description of the Ncar Community Atmosphere Model (cam 3.0). *NCAR Tech. Note NCAR/TN-464 STR* **2004**, *226*, 1–200.
53. Dee, D.P.; Uppala, S.M.; Simmons, A.J.; Berrisford, P.; Poli, P.; Kobayashi, S.; Andrae, U.; Balmaseda, M.A.; Balsamo, G.; Bauer, P. The Era-Interim Reanalysis: Configuration and Performance of the Data Assimilation System. *Quart. J. R. Meteorol. Soc.* **2011**, *137*, 553–597. [CrossRef]
54. Rydsaa, J.; Stordal, F.; Tallaksen, L. Sensitivity of the Regional European Boreal Climate to Changes in Surface Properties Resulting from Structural Vegetation Perturbations. *Biogeosciences* **2015**, *12*, 3071–3087. [CrossRef]
55. Cao, Q.; Yu, D.Y.; Georgescu, M.; Han, Z.; Wu, J.G. Zy-Impacts of Land Use and Land Cover Change on Regional Climate: A Case Study in the Agro-Pastoral Transitional Zone of China. *Environ. Res. Lett.* **2015**, *10*, 124025. [CrossRef]
56. Zhang, M.; Ma, M.; De Maeyer, P.; Kurban, A. Uncertainties in Classification System Conversion and an Analysis of Inconsistencies in Global Land Cover Products. *ISPRS Int. J. Geo-Inf.* **2017**, *6*, 112. [CrossRef]
57. Chen, X. *Land Use/Cover Change in Arid Area in China*; Ke Xue Chu Ban She: Beijing, China, 2008.
58. Miller, J.; Barlage, M.; Zeng, X.; Wei, H.; Mitchell, K.; Tarpley, D. Sensitivity of the Ncep/Noah Land Surface Model to the Modis Green Vegetation Fraction Data Set. *Geophys. Res. Lett.* **2006**, *33*. [CrossRef]
59. Lim, Y.-J.; Hong, J.; Lee, T.-Y. Spin-up Behavior of Soil Moisture Content over East Asia in a Land Surface Model. *Meteorol. Atmos. Phys.* **2012**, *118*, 151–161. [CrossRef]
60. Kumar, A.; Chen, F.; Barlage, M.; Ek, M.B.; Niyogi, D. Assessing Impacts of Integrating Modis Vegetation Data in the Weather Research and Forecasting (WRF) Model Coupled to Two Different Canopy-Resistance Approaches. *J. Appl. Meteorol.* **2014**, *53*, 1362–1380. [CrossRef]
61. Zhang, C.; Fan, G.; Ma, Z.; Cheng, B.; Zhao, B.; Feng, J.; Wang, H. Characteristics of Albedo over Different Underlying Surface in the Semi-Arid Area. *Plateau Meteorol.* **2015**, *34*, 11.
62. Litan, S.; Shalamu, A.; Yu-dong, S. Effects of Drip irrigation Volume on Soil Water-Salt Transfer and Its Redistribution. *Arid Zone Res.* **2011**, *1*, 13.

63. Zhang, L.; Jiang, P.; Wu, H.; Li, M. Research on Spectral Characteristics of Typical Soil in North Xinjiang. *J. Soil Water Conserv.* **2013**, *1*, 4.
64. Liu, X.; Tian, C. Study on Dynamic and Balance of Salt for Cotton under Plastic Mulch in South Xinjiang. *J. Soil Water Conserv.* **2005**, *6*, 20.
65. Hanna, S.R.; Yang, R.X. Evaluations of Mesoscale Models' Simulations of Near-Surface Winds, Temperature Gradients and Mixing Depths. *J. Appl. Meteorol.* **2001**, *40*, 1095–1104. [CrossRef]
66. Whiteman, C.D. *Mountain Meteorology: Fundamentals and Applications*; Oxford University Press: Oxford, UK, 2000.
67. Long, Z.P. *Analysis of Dry and Wet Change in Northwest China in Recent 700 Years*; Lanzhou University: Lanzhou, China, 2015.